25,000 Years Long Seismic Cycle in a Slow Deforming Continental Region of Mongolia

Laurent Bollinger (laurent.bollinger@cea.fr)
CEA DAM Île-de-France
Yann Klinger
Institut De Physique Du Globe De Paris
Steven Forman
Baylor University
Odonbaatar Chimed
Institute of Astronomy and Geophysics
Amgalan Bayasgalan
Mongolian University of Science and Technology
Ulziibat Munkhuu
Institute of Astronomy and Geophysics
Ganzorig Davaasuren
Institute of Astronomy and Geophysics
Tulga Dolgorsuren
Institute of Astronomy and Geophysics
Bayarsaikhan Enkhee
Institute of Astronomy and Geophysics
Demberel Sodnomsambuu
Institute of Astronomy and Geophysics

Research Article

Keywords: Slowly Deforming Continental Regions (SDCR), faster deforming regions, seismogenic sources, seismic hazard models

Posted Date: March 18th, 2021

DOI: https://doi.org/10.21203/rs.3.rs-310793/v1

25,000 Years Long Seismic Cycle in a Slow Deforming Continental Region of Mongolia

Laurent Bollinger[1,*], Yann Klinger[2], Steven L. Forman[3], Odonbaatar Chimed [4], Amgalan Bayasgalan[5], Ulziibat Munkhuu[4], Ganzorig Davaasuren[4], Tulga Dolgorsuren[4], Bayarsaikhan Enkhee[4], Demberel Sodnomsambuu[4]

1-CEA, DAM, DIF, Arpajon, France
2-Université de Paris, Institut de physique du globe de Paris, CNRS, Paris, France.
3-Geoluminescence Dating Research Laboratory, Department of Geosciences, Baylor University, One Bear Place, Waco, TX 76798, USA
4-Institute of Astronomy and Geophysics, Ulaanbaatar, Mongolia
5-Mongolian University of Science and Technology, Ulaanbaatar, Mongolia

*corresponding author: Laurent.bollinger@cea.fr

Abstract

The spatial distribution of large earthquakes in Slowly Deforming Continental Regions (SDCR) is poorly documented and, thus, has often been deemed to be random. Unlike in high strain regions, where seismic activity concentrates cyclically along major active faults, earthquakes in SDCR may seem to occur more erratically in space and time. This questions classical fault behavior models, posing paramount issues for seismic hazard assessment. Here, we investigate the M7, 1967, Mogod earthquake in Mongolia, a region recognized as a SDCR. Despite the absence of visible cumulative deformation at the ground surface, we found evidence for at least 3 surface rupturing earthquakes during the last 50,000 years, associated to a slip-rate of 0,06 ± 0,01 mm/yr. These results show that in SDCR, like in faster deforming regions, deformation localizes on specific structures. However, the excessive length of return time for large earthquakes along these structures makes it more difficult to recognize earthquake series, and could conversely lead to the misconception that in SDCR earthquakes would be randomly located. Thus, our result emphasizes the need for systematic appraisal of the potential seismogenic structures in SDCR in order to lower the uncertainties associated with the seismogenic sources in seismic hazard models.

INTRODUCTION – SEISMOTECTONIC SETTING

The seismic behavior of faults in slowly deforming continental regions (SDCR) is a major source of uncertainty for seismic hazard assessment (e.g. 1). Slow-slipping faults show a variety of earthquake behaviors ranging from periodic seismicity to complex behavior alternating periods of clustered activity with seismic quiescence (e.g. 2, 3). In fact, it has been suggested that for some of the slowest slipping faults a single earthquake could occur with no distinguishable repeat pattern nor cumulative scarps[1]. These drastically different fault behaviors have been previously related to differences in loading rate, strength, healing rate, and interactions with external stressing rate, including the effects of lithospheric response to surface loads (e.g. 4-7) and fault interactions within a spatial cluster of events. (e.g. 8-9).

One major limitation in ascertaining which seismic behavior model might be most appropriate for SDCR is the limited number of paleoseismological sites recording a period long enough, from 10^4 to 10^5 years, to include a significant series of earthquakes. In many cases, only one or two events are identified, making it difficult to examine the behavior of faults over multiple seismic cycles (e.g. in 10).

Mongolia is such an intracontinental region. To the west of Hangay dome, a broad high-elevation low-relief topography in central-western Mongolia (Fig. 1), large strike-slip faults have been recognized that are accommodating the northernmost part of the India-Eurasia collision[11]. Based on geologic and geodetic records, the slip rate on these different faults is estimated to be in the range of 1-3 mm/yr (e.g. 12-13). The stress build up related to this deformation is released by some moderate background seismicity, in addition to unusually large M8 strike-slip earthquakes, which seem to happen in temporal clusters triggered by postseismic viscoelastic stress transfer[8,9]. These large earthquakes have left spectacular surface ruptures scars along the principal fault systems including the Bolnai, Hovd, and Gobi-Altai systems[14-17] (Fig. 1). Further North, the Baikal rift system accommodates localized

extension at velocities locally larger than 3mm/yr (ref. 18-20). In contrast, the deformation appears more distributed in the Hangay dome[21] , a region where faults are sometimes only evidenced by the seismic activity [22-23].

The areas of central and eastern Mongolia, east of the Hangay dome (Fig. 1), are characterized by a low seismicity, that often occurs during seismic swarms[24]. Fault slip rates, localization and recurrence for large earthquakes remain mostly unknown in this part of Mongolia, usually described as a part of the Amurian plate, and recognized as a SDCR[25]. Indeed, the boundaries of the Amurian plate remain controversial due to the low seismicity rate, distributed faulting (e.g. 26-29), and very low rates of deformation, $\leq 2.10^{-8}$ yrs^{-1} (ref. 30-31).

The 1967 Mogod earthquake

The January 5th, 1967 Mogod earthquake happened along the north-eastern edge of the Hangay dome (Fig. 1). The seismic source of the Mw 7.1 earthquake was extensively studied using both seismological and field observations[32-34]. Indeed, the earthquake surface rupture is about 40 km-long with numerous co-seismic displacements larger than one meter[34-37]. The surface trace comprises three principal fault sections and dozens of secondary structures. Waveform inversions revealed that the earthquake could be decomposed in three seismic sub-events, which focal mechanism, magnitude, and location are consistent with the three surface rupture sections[33, 34]. The two northernmost fault sections are mainly North-South dextral strike-slip faults, that ruptured along the western edge of the *Mogodyn Nuruu* mountain ridge (Fig. 1). The second sub-event ruptured the central segment, generating mole tracks and tension cracks across the topography of a second ridge, the *Burdiin Hyar Uul* (Fig. 1). In contrast, the third section corresponds to a thrust fault, which produced a surface rupture that follows the SE-NW trending ridge of *Tüleet Uul* (Fig. 1).

The geomorphic expression of the rupture is changing along strike, with the rupture trace probably being controlled by inherited structures at depth, enforcing segmentation of the fault system. The morphology of the ruptures at the junction between the central strike-slip section and the southern thrust section is complex, including two parallel reverse faults, which have clear surface rupture expression, in addition to many secondary ruptures. The southernmost reverse scarp is located at the base of a large slope, facing up-slope and blocking sediments that go down the subdued drainage colleting surface wash (Fig. 1b, 2). This southwest-facing scarp is ~1 meter-high, with some lateral variations. The southeastern end of the scarp is well marked with the rupture reaching to the surface (Fig. 2). Conversely, the morphology of the scarp is smoother further west, where the main fault is blind and the rupture is more characterized by a flexural scarp. However, parallel to the flexural scarp, north of it, a secondary 10 to 20 cm-high northeasterly facing scarplet is visible, which developed above a backthrust.

PALEOSEISMOLOGICAL TRENCH

We excavated a 20 m-long 2.5 m-deep trench at the *Tület Uul* site. The geological units exposed on the trench walls include fluvial and aeolian sediments, as well as metamorphic bedrock. The fluvial sediments are fine, medium, and coarse sands, sometimes interbedded with matrix-supported gravels. The two walls were mapped in detail and were subdivided into nine units based on lithology and geometry (Fig. 3). Although the main fault zone is not visible in the trench, a backthrust branching off the main fault below the trench bottom reaches the ground surface. This backthrust, dipping 25° southward, is outlined by a reddish, gouge-rich, shear zone that forms a thrust sole that can exceed 20 cm in thickness. All units visible in the trench are affected by this backthrust. Hence, they have been labeled UxN and UxS for units located respectively in the footwall and hangingwall of the backthrust. Locally, dragging and folding of the different units of the footwall, including some gouge reworked by

the fault are visible, such as at the southern end of U2N, attesting of successive earthquakes.

The sedimentary units U1 to U3 can be found on both sides of the backthrust. South of the backthrust, in the hanging wall, the three units thicken gradually away from the scarp, following a growth strata geometry. Closer to the scarp, units onlap unconformably on top of each other along erosional contacts marked by coarser material. The successive dip angles change from 3° towards the south at the top of U0S, to 6° S between U2S and U3S, and 13° S between U3S and U4S, indicating incremental tilting.

North of the backthrust, in the footwall, the top layers are formed by fine sediments U1N and U2N, almost identical to sediments across the fault. Below these units sits a fluvial unit, U3N, formed by coarse gravel to pebble in a sandy matrix that eroded in the shattered bedrock that forms the lower part of the wall.

This unit is itself incised by 2 channels characterized by pebble and cobbles, which obliterate parts of the stratigraphic relations between the successive sedimentary units. The different sedimentary units are consistently separated by a few cm-thick red layer that is interpreted to be some gouge-derived clay washed away from the fault zone along what was at that time the ground surface. This red clay is also found on top of the two channels, although stratigraphy has obviously been locally perturbed during emplacement of channels, and it is likely that the red clay that currently overlays the two channels has been remobilized one or several times, hence its complex depositional facies.

The fault zone is characterized by a red-color shear zone that thickens downward, becoming more complex towards the base of the trench. Several folded layers and sheared chunks of bedrock have been incorporated into the fault zone, attesting of intense deformation, likely associated with numerous earthquakes.

Eventually, the emplacement of each sedimentary unit U1S to U3S is interpreted to relate to rejuvenation of the flexural scarp during successive earthquakes that would dam the incoming

sediments. Concomitantly, more gouge-derived clay would be washed away northward soon after the backthrust break to the surface. Thus, our trench exposure suggests that there is evidence for at least three ground-breaking events at the *Tület Uul* trench site, including the 1967 Mogod earthquake.

AGE CONTROL ON PALEO-EARTHQUAKE OCCURENCES

The earthquake horizon that corresponds to the most recent earthquake in 1967 is the actual ground surface, where surface ruptures are still visible, suggesting that under the current climatic conditions both sedimentation and erosion rates are very low. Dating older units has proved difficult, as sediments are mostly devoid of any organic material usable for radiocarbon dating. Thus, 7 samples were collected in order to perform Optically Stimulated Luminescence (OSL) dating on sandy material.

Samples were collected by embedding 100 mm-long opaque metallic tubes into cleaned sections of trench walls. In addition, bag samples were collected from around the OSL sample to determine the local dose rate, mineralogy, and particle size. The samples were then processed for OSL dating, following [38] and analytical approaches as in [39](see also sup. mat.). In most cases, dispersion of the equivalent dose *De* is 30% or larger. Such large dispersion might be due to different factors, including partial bleaching and mixing of the material. We therefore discuss ages considering a minimum age model (see sup. mat. for justification of such strategy).The seven dates distribute over a period from 17 ka to >81 ka, spanning the last glacial period (Table 1; Fig. 3).

At first order the stratigraphic order of ages fits the sample depth. OSL7 and OSL6 were sampled in unit U1S, the highest fine-sediments unit sampled for OSL, that yield consistent minimum ages of 17 ± 2 ka. OSL1 and OSL2 were sampled in well-defined clean sand pockets in U2S. These sandy pockets correspond to rill channels flowing along the scarp

158 before this space in front of the scarp get filled with new sediments. These two samples give
159 consistent ages of respectively 50±5 and 58±3 ka. OSL3, collected in unit U3S, yields an age
160 > 81 ka. OSL5 was sampled north of the backthrust in a unit which stratigraphic relation to
161 the top units is obscured by successive channeling. Its age of 55±7 ka is similar to the age of
162 OSL1 and OSL2, suggesting that this unit would be U2N, a lateral equivalent to unit U2S.
163 This is a reasonable assumption in view of its stratigraphic position, slightly higher than the
164 transition from yellowish fine to medium silty sand with few gravels to the coarser sandy
165 gravel, almost clast supported unit, more greyish in color, which might be a lateral equivalent
166 of U3. OSL4 was sampled closer to the fault, in U2N. It yields an age >65 ka. Although we
167 could not totally disregard this age, similarly to OSL3 this sample was far from ideal, as it
168 was sampled in a rather heterogeneous drag fold hinge. Several factors might have biased age
169 determination such as limited amount of datable material, sample saturation, or partial
170 bleaching issues (see sup. mat. for a complete report about OS3 and OS4 measurements).
171 Hence, interpretation of this age should be handled cautiously.
172
173 **DISCUSSION**
174 Based on our trench exposure, we can propose a systematic earthquake-deformation scenario
175 that repeated at least three times, including in 1967, and led to the current outcrop
176 configuration (Fig. 4).
177 During each earthquake, the blind thrust is activated that rejuvenates the main flexural scarp
178 and uplifts the hanging wall by about 1 meter (Fig. 2c). Similarly, the backthrust is also
179 activated in the hanging wall, breaking to the surface. Up-slope fine-grained material,
180 destabilized by earthquake ground shaking, quickly accumulates in front of the flexural scarp,
181 which is facing mountain slope, transported either by wind or by surface wash. Some of the
182 newly created scarp is also eroded, contributing as well to level off the trough in front of the

183 scarp. At the same time, gouge-derived red clay is rinsed off from backthrust surface rupture
184 and gets redeposited nearby on the ground surface.
185 Thus, the fault-related topography ends up being partly eroded and eventually buried by
186 sediments coming down the slope of the mountain range. During the next earthquake, existing
187 sediments get tilted and new sediments are deposited onlapping unconformably on top of
188 older ones. The contact between these two sediment bodies combined with the thin clay layer,
189 north of the backthrust, defines an earthquake horizon.
190 The last earthquake, in 1967, tilted the unit U1S about 3° southward. Based on OSL6 and
191 OSL7 ages about 17±2 ka, and assuming that post-earthquake sediments get emplaced soon
192 after the earthquake, in a couple of thousands of years, when destabilized sediments are most
193 available, we propose that the penultimate event, Eq2, happened about 20-25 ka ago. The
194 contact between U1S et U2S is tilted about 6° southward, roughly twice the tilt associated to
195 the 1967 event, suggesting that locally the deformation was about the same amplitude. Based
196 on samples OSL1, OSL2, and OSL5, and following the same reasoning as before, we propose
197 that Eq3 happened about 55 ka to 60 ka ago. Indeed, such scenario implies that for some
198 reason, not yet well understood, OSL4 gives an age older than the true deposition age. The
199 existence of distinct steeply dipping matrix supported gravel beds at the base of U3S, next to
200 the fault plane, and of a similar looking unit making an erosional contact on top of US4, north
201 of the fault plane, suggest that a fourth event might be recorded in this trench. Hence, based
202 on OSL3 this event would have happened more than 81 ka ago. Evidence for this fourth
203 event, however, remains faint.
204 Indeed, age constrains in this trench only allow for a first order earthquake timing. However,
205 assuming a systematic quick post-earthquake sedimentation across the scarp, and based on the
206 ages available, our observation suggests that 3 to 4 Mogod-style earthquakes occurred on that
207 fault, each time separated by 20 ka to 30 ka.

The exact amount of slip on the main blind thrust during the 1967 event remains unknown. However, considering the vertical deformation of the flexural scarp, ~1 m, and that about 10 cm to 20 cm of slip was accommodated by the backthrust, the total slip on the fault at depth cannot exceed about 1.5 m, independently of the fault dip at depth. Indeed, this is consistent with what was documented in the field[34].

Thus, combining a first order return time for Mogod-style event of 25 ± 5 ka with a maximum slip of 1.5 m per event leads to a maximum slip rate on the Mogod fault of about 0.06 ± 0.01 mm/yr estimated over several tens of thousands of years. This rate, which represents an upper bound, remains under the current detection threshold of geodesy.

Implications for earthquake processes and hazard assessment in SDCR

The *Tület Uul* trench shows evidence for three to four earthquakes on the same structure, despite the absence of visible cumulative deformation in the surficial geomorphology. The return time for Mogod-style earthquakes is on the order of a few tens of thousands of years. Thus, significant variations in climatic conditions have occurred between successive earthquakes, including the end of the last glacial period between the 1967 earthquake and the penultimate earthquake. Climatic conditions during the time period covered by our paleoseismological record include several episodes colder and more arid than today, during the last glacial period (e.g. 40). Few warmer and wetter periods are also documented. Hence, in addition to the typical diffusion erosion process that affects scarps everywhere through out Asia[41], local erosional processes have likely been temporary emphasized by climatic changes. Eventually, given the very long time interval between successive earthquakes along the Mogod fault, and the small size of the co-seismic fault escarpment, these processes resulted in eroding evidence of previous surface ruptures and prevented the building of obvious significant cumulative scarps.

232 This is not specific to the Mogod earthquake area, and similar difficulties to find well-
233 preserved Quaternary cumulative deformation have been reported elsewhere in central and
234 northern Mongolia (e.g. 42, 14, 16). This trench, however, demonstrates that even in SDCR
235 with low rates of deformation, the deformation could localize on specific structures where
236 deformation is accommodated through successive earthquake cycles despite the absence of
237 visible cumulative scarps. In fact, absence of cumulative topography makes it difficult to
238 assess the actual length of the fault structure beyond the section that did rupture most recently.
239 Hence, it suggests that in SDCR a special attention should be paid in localizing such fault
240 zones and trying to describe longer paleoearthquake time series (e.g. ref. 43-46), as they bear
241 special significance in term of assessing seismic hazard.
242 In the case of Mongolia, the Mogod earthquake came in 1967, at the end of an earthquake
243 sequence that ruptured 4 major faults during 4 magnitude M8 earthquakes, between 1905 and
244 1957 [14, 16, 17, 46-49]. All together, these 4 events released in about 50 years the stress equivalent
245 to a loading rate of 50mm/yr (ref. 50), about 6 times what is actually measured by geodesy
246 across Mongolia [12]. Thus, it has been proposed that this unusual sequence resulted from
247 specific fault interactions and visco-elastic relaxation effects of one event that would lead to
248 trigger the next one[8, 9], ending up in a major spatio-temporal cluster of event. The question of
249 existence of similar earthquake clusters earlier in time remains unsolved yet. At best, it has
250 been shown that return time for M8 earthquakes along the Bulnai fault is on the order of 3 ka
251 to 4 ka[14]. Similar time scale has been suggested for the Fuyun fault[46] although timing is
252 poorly constrained. Our trench shows that Mogod-style earthquakes follow a different pattern
253 with a repeat time of the order of several tens of thousands of years. The XXth century
254 earthquake cluster in western central Mongolia, however, has certainly contributed to the
255 loading the Mogod fault and might have hastened the Mogod earthquake. Hence, it
256 emphasizes that for active faults with low loading rate, the contribution to fault loading of far

seismic sources could be more significant than in faster deforming regions, where long-term tectonic loading dominates, and should therefore be considered thoroughly in SDCR seismic hazard assessment.

ACKNOWLEDGEMENTS :

This work was partly funded by Institute of Astronomy and Geophysics (IAG), Ulan Bator, Mongolia. LB benefited from additional funding from CEA/DASE, France. YK benefited from additional funding from ANR-12-BS06-0016 contract.

We are grateful to the IAG for organizing the project and field excursion for the 50th anniversary of the earthquake. We also thank Antoine Schlupp for sharing his previous works on the Mogod fault, as well as Battogtokh Davaasambuu for fruitfull discussions. We thank Christoph Grützner and an anonymous reviewer for their comments on a previous version of this article.

Author contributions:

Y.K., L.B., O.B., A.B., U.M., G.D., T.D., B.E., D.S. organised and/or conducted the fieldwork. S.F. conducted the OSL laboratory analyses. All authors exchanged on the results and implications. L.B. and Y.K wrote the manuscript with contributions from SF.

Additional information

Supplementary information, concerning OSL dating, is available in the online version of the paper. Reprints and permissions information is available online at www.nature.com/reprints. Correspondence and requests for materials should be addressed to L.B.

Competing interests:

The authors declare no competing interests.

References :

1. Calais, E., Camelbeeck, T., Stein, S., Liu, M., & Craig, T. J. A new paradigm for large earthquakes in stable continental plate interiors. *Geophys. Res. Lett.*, **43**(20) (2016).

2. Crone, A. J., Machette, M. N., & Bowman, J. R. Episodic nature of earthquake activity in stable continental regions revealed by palaeoseismicity studies of Australian and North American Quaternary faults. *Australian Journal of Earth Sciences* **44** (2), 203-214 (1997).

3. Clark, D., McPherson, A., & Van Dissen, R. Long-term behaviour of Australian stable continental region (SCR) faults. *Tectonophysics*, **566**, 1-30 (2012).

4. Hampel, A., & Hetzel, R. Response of normal faults to glacial-interglacial fluctuations of ice and water masses on Earth's surface. *J. Geophys. Res.: Solid Earth* **111**B6) (2006).

5. Luttrell, K., & Sandwell, D. Ocean loading effects on stress at near shore plate boundary fault systems. *Jour. Geophys. Res.: Solid Earth* **115** B8 (2010).

6. Craig, T. J., Calais, E., Fleitout, L., Bollinger, L., & Scotti, O. Evidence for the release of long-term tectonic strain stored in continental interiors through intraplate earthquakes. *Geophys. Res. Lett.* **43** (13), 6826-6836 (2016).

7. Brandes, C., Steffen, H., Steffen, R., & Wu, P. Intraplate seismicity in northern Central Europe is induced by the last glaciation. *Geology* **43** (7), 611-614 (2015).

8. Chery, J., Carretier, S., & Ritz, J. F. Postseismic stress transfer explains time clustering of large earthquakes in Mongolia. *Earth and Planetary Science Letters* **194** (1-2), 277-286 (2001).

9. Pollitz, F., M. Vergnolle & Calais E. Fault Interaction and Stress Triggering of Twentieth Century Earthquakes in Mongolia: stress triggering of earthquakes in mongolia. *J.Geophys. Res.: Solid Earth* **108** (B10). doi:10.1029/2002JB002375 (2003).

10. Whitney, B. & Hengesh J. Assessing the “Clustering and Quiescence” earthquake occurrence model fo Stable Continental Region faults and the implications for Probabilistic Seismic Hazard Analysis, 8th international INQUA meeting on paleoseismology, active tectonics and archeoseismology (PATA), 13-16 november 2017, New Zealand, November 2017, 432-436 (2017).

11. Tapponnier, P., & Molnar, P. Active faulting and Cenozoic tectonics of the Tien Shan, Mongolia, and Baykal regions. *J. Geophys. Res.*, **84** (B7), 3425-3459 (1979).

12. Calais, E., M. Vergnolle, V. San'kov, A. Lukhnev, A. Miroshnitchenko, S. Amarajargal & Deverchère J. GPS measurements of crustal déformation in the Baikal-Mongolia area (1994-2002) : Implications for current kinematics of Asia, *J. Geophys.Res.: Solid Earth* **108** (B10) https://doi.org/10.1029/2002JB002373 (2003).

13. Ritz , J.F. et al. Late pléistocène to Holocene slip rates for the Gurvan Bulag thrust fault (Gobi-Altay, Mongolia) estimated with 10Be dates, *J. Geophys. Res.*, **108** (B3) (2003).

14. Rizza, M., Ritz, J.F., Prentice, C. et al. Earthquake geology of the Bulnay fault (Mongolia). *Bull. Seismo. Soc. Am.*, **105** (1), 72-93 (2015).

15. Schlupp, A. & A. Cisternas Source history of the 1905 great Mongolian earthquakes (Tsetserleg, Bolnay), *Geophys. Jour. Int.*, **169** (3), 1115-1131 (2007).

16. Choi, J. H., Klinger, Y., Ferry, M., Ritz, J. F., Kurtz, R., Rizza, M., Bollinger, L. , Davaasambuu, B., Tsend-Ayush, N. & Demberel, S. Geologic inheritance and earthquake rupture processes: the 1905 M≥ 8 Tsetserleg-Bulnay strike-slip earthquake sequence, Mongolia. *J. Geophys. Res.*, 10.1002/2017JB013962.zz (2018).

17. Kurtz, R., Klinger, Y., Ferry, M., & Ritz, J. F. Horizontal surface-slip distribution through several seismic cycles: The Eastern Bogd fault, Gobi-Altai, Mongolia. *Tectonophysics* **734**, 167-182 (2018).

18. Calais, E., Vergnolle, M., San'Kov, V., Lukhnev, A., Miroshnitchenko, A., Amarjargal, S., & Déverchère, J. GPS measurements of crustal deformation in the Baikal-Mongolia area (1994–2002): Implications for current kinematics of Asia. *J. Geophys. Res.: Solid Earth,* **108**(B10) (2003).

19. Sankov, V. A., Lukhnev, A. V., Miroshnitchenko, A. I., Dobrynina, A. A., Ashurkov, S. V., Byzov, L. M., ... & Déverchère, J. Contemporary horizontal movements and seismicity of the south Baikal Basin (Baikal rift system). *Izvestiya, Physics of the Solid Earth*, **50**(6), 785-794 (2014).

20. Ritz, J. F., Arzhannikova, A., Vassallo, R., Arzhannikov, S., Larroque, C., Michelot, J. L., & Massault, M. Characterizing the Present-Day Activity of the Tunka and Sayan Faults Within Their Relay Zone (Western Baikal Rift System, Russia). *Tectonics*, **37**(5), 1376-1392 (2018).

21. Walker, R. T., Molor, E. , Fox, M. & Bayasgalan, A. Active tectonics of an apparently aseismic region: distributed active strike-slip faulting in the Hangay Mountains of central Mongolia. *Geophysical Journal International*, **174**, 3, 1121-1137 (2008).

22. Meltzer, A., Stachnik, J. C., Sodnomsambuu, D., Munkhuu, U., Tsagaan, B., Dashdondog, M., & Russo, R. The Central Mongolia seismic experiment: multiple applications of temporary broadband seismic arrays. *Seismological Research Letters*, **90**(3), 1364-1376 (2019).

342 23. Dashdondog, M., Chimed, O., Meltzer, A., Erdenetsogt, N. E., & Stachnik, J. Determining 1D velocity
343 model from local earthquake data in the South Hangay region, central Mongolia. *Proceedings of the Mongolian*
344 *Academy of Sciences*, 1-14 (2020).
345 24. Adiya, M. Seismic activity near Ulannbaatar: implication for seismic hazard assessment (Doctoral
346 dissertation, Université de strasbourg) (2016).
347 25. Johnston, A. C., Coppersmith, K. J., Kanter, L.R. & Cornell, C.A. The earthquakes of stable continental
348 regions: assessment of large earthquake potential, TR-102261, Vol. 1–5, ed. Schneider, J.F., Electric Power
349 Research Institute (EPRI), Palo Alto, CA. (1994).
350 26. Ferry, M., Schlupp, A., Ulzibat, M., Munschy, M., Fleury, S., Baatarsuren, G., ... & Ankhtsetseg, D.
351 Tectonic morphology of the Hustai fault (Northern Mongolia): a source of seismic hazard for the city of
352 Ulaanbaatar. *EGUGA*, 11122, (2010).
353 27. Schlupp, A., Ferry, M. A., Munkhuu, U., Munschy, M., & Fleury, S. Tectonic Morphology of the
354 Hustai Fault (Northern Mongolia): Implications for Regional Geodynamics. *AGUFM*, *2010*, T23D-08 (2010).
355 28. Smekalin, O. P., Imaev, V. S., & Chipizubov, A. V. Paleoseismic studies of the Hustai Fault zone
356 (Northern Mongolia). *Russian Geology and Geophysics*, *54*(7), 724-733 (2013).
357 29. Suzuki, Y., Nakata, T., Watanabe, M., Battulga, S., Enkhtaivan, D., Demberel, S., ... & Badral, T.
358 Discovery of Ulaanbaatar Fault: A New Earthquake Threat to the Capital of Mongolia. *Seismological Society of*
359 *America*, *92*(1), 437-447 (2021).
360 30. Lukhnev, A. V., San'kov, V. A., Miroshnichenko, A. I., Ashurkov, S. V., & Calais, E. GPS rotation and
361 strain rates in the Baikal–Mongolia region. *Russian Geology and Geophysics*, **51**(7), 785-793 (2010).
362 31. Ashurkov, S. V., San'Kov, V. A., Serov, M. A., Luk'yanov, P. Y., Grib, N. N., Bordonskii, G. S., &
363 Dembelov, M. G. Evaluation of present-day deformations in the Amurian Plate and its surroundings, based on
364 GPS data. *Russian Geology and Geophysics*, **57**(11), 1626-1634 (2016).
365 32. Okal, E.A. A surface-wave investigation of the rupture mechanism of the Gobi-Altai (December 4,
366 1957) earthquake, *Phys. Earth Planet. Inter.*, **12**, 319-328 (1976).
367 33. Huang, J., & Chen, W. P. Source mechanisms of the Mogod earthquake sequence of 1967 and the event
368 of 1974 July 4 in Mongolia. *Geophysical Journal of the Royal Astronomical Society*, **84**(2), 361-379 (1986).
369 34. Bayasgalan, A. & Jackson, J. A re-assessment of the faulting in the 1967 Mogod earthquakes in
370 Mongolia, Geophys. Jour. Int., 138, 784-800 (1999).

35. Natsag-Yüm, L., Baljinnyam, I. & Monhoo, D. Mongolian earthquakes, in Seismic regionalization of Ulan Bator, 54-82, *Nauka*, Moscow (in Russian) (1971).

36. Khil'ko, S., Kurushin, R.A…. Strong earthquakes, paleosismological and macroseismic data, **41**, 19-83 (1985).

37. Rogozhin, E. A., Imaev, V. S., Smekalin, O. P. & Schwartz, D. P. Tectonic position and geological manifestations of the Mogod (Central Mongolia), January 5, 1967, earthquake (a view after 40 years). *Izvestiya, Physics of the Solid Earth* **44** (8), 666-677 (2008).

38. Forman, S.L., Tripaldi & A. Ciccioli, P.L. Sand sheet deposition in the San Luis paleodune field, western Argentina as an indicator of a semi-arid environment through the Holocene. *Paleogeography, Paleoclimatology, Paleoecology* **411**, 122-135 (2014).

39. Liang, P. & Forman, S. L. LDAC: an Excel-based program for luminescence equivalent dose and burial age calculations. *Ancient TL* **37**, 21-40 (2019).

40. Zwyns, N., Paine, C. H., Tsedendorj, B., Talamo, S., Fitzsimmons, K. E., Gantumur, A., ... & Hublin, J. J. The northern Route for Human dispersal in central and northeast Asia: new evidence from the site of Tolbor-16, Mongolia. *Scientific reports*, **9**(1), 1-10 (2019).

41. Avouac, J. P. Analysis of scarp profiles: evaluation of errors in morphologic dating. *Journal of Geophysical Research: Solid Earth*, *98*(B4), 6745-6754 (1993).

42. Walker, R.T., Bayasgalan, A., Carson, R., Hazlett, R., McCarthy, L., Mischler, J., Molor, E., Sarantsetseg, P., Smith, L., Tsogtbadrakh, B. & Tsolmon, G. Geomorphology and structure of the Jid right-lateral strike-slip fault in the Mongolian Altay mountains. *Journal of Structural Geology*, 28, 1607–1622, doi: 10.1016/j.jsg.2006.04.007 (2006).

43. Campbell, G. E., Walker, R. T., Abdrakhmatov, K., Jackson, J., Elliott, J. R., Mackenzie, D., ... & Schwenninger, J. L. Great earthquakes in low strain rate continental interiors: an example from SE Kazakhstan. *Journal of Geophysical Research: Solid Earth*, **120**(8), 5507-5534 (2015).

44. Copley, A., Mitra, S., Sloan, R. A. , & Gaonkar, S. Active faulting in apparently stable peninsular India: Rift inversion and a Holocene-age great earthquake on the Tapti Fault, *Journal of Geophysical Research: Solid Earth*, **119** (8), 6650-6666 (2014).

45. Vanneste, K., Camelbeeck, T. & Verbeeck K. A model of composite seismic sources for the Lower Rhine Graben, Northwest Europe. Bulletin of the Seismological Society of America 103.2A (2013): 984-1007.

46. Klinger Y., Etchebes M., Tapponnier P & Narteau C. Characteristic slip for five great earthquakes along the Fuyun fault in China. *Nature Geoscience*, **4**, 389-392, doi:10.1038/ngeo1158 (2011).

47. Prentice, C. et al. Prehistoric Ruptures of the Gurvan Bulag Fault, Gobi Altay, Mongolia. *Journal of Geophysical Research* **107** (B12). https://doi.org/10.1029/2001JB000803 (2002).

48. Schwartz, D. P. et al. The 1957 Gobi-Altay earthquake (M= 8.1); complex: long recurrence (?) interval faulting in the middle of a continent. *Seismol. Res. Lett* **67**:54 (1996).

49. van der Wal, J. L., Nottebaum, V. C., Gailleton, B., Stauch, G., Weismüller, C., Batkhishig, O., ... & Reicherter, K. Morphotectonics of the northern Bogd fault and implications for Middle Pleistocene to modern uplift rates in southern Mongolia. Geomorphology, 367, 107330 (2020).

50. Baljinnyam, I et al. Ruptures of major earthquakes and active déformation in Mongolia and its surroundings , *Geol. Soc. Am. Mem.*, 181 (1993).

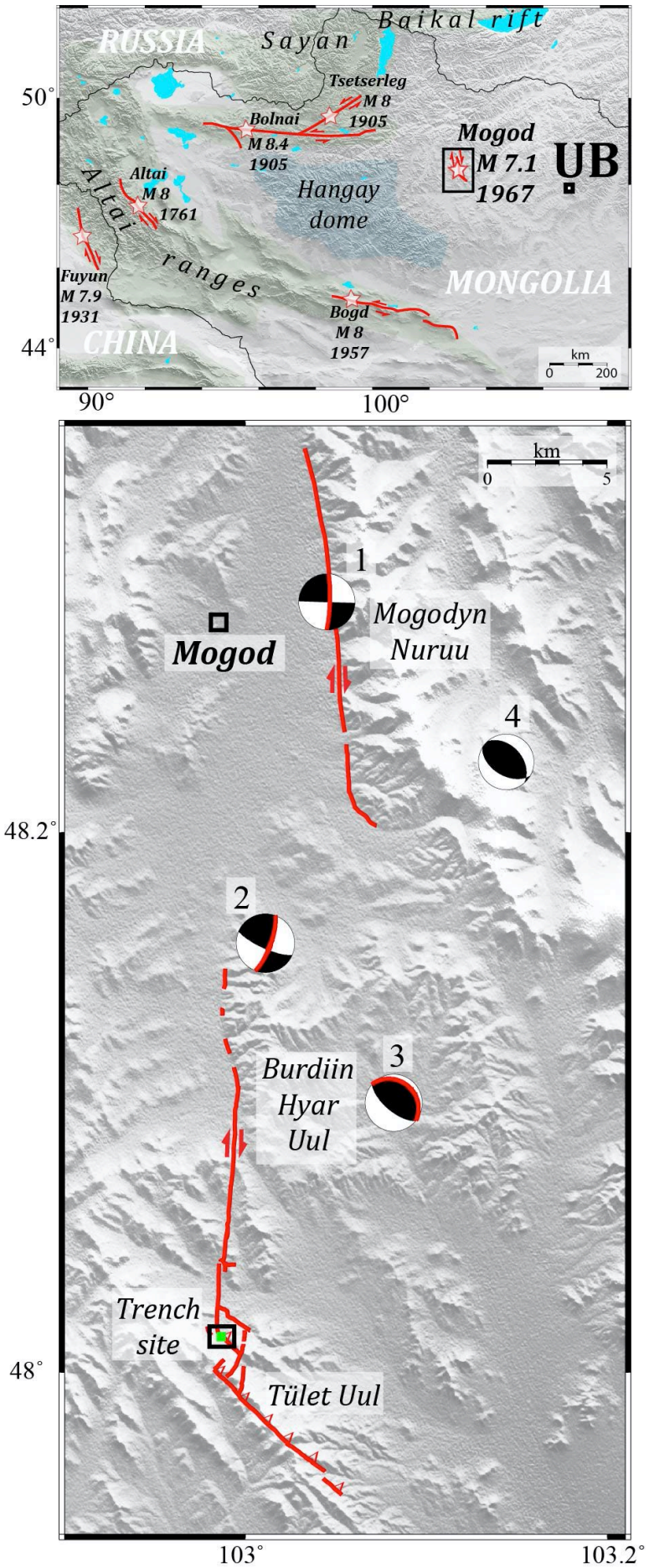

Figure 1: (Top) Map of the large surface rupturing earthquakes of the last 300 years in Mongolia and vicinity. (Bottom) Surface trace of the 1967CE rupture surveyed from high resolution images. Centroid Moment Tensors from Bayasgalan and Jackson, 1999. (1-2-3) label the 3 subsources of the Main shock. (4) is the largest aftershock that occurred on January the 20th 1967.

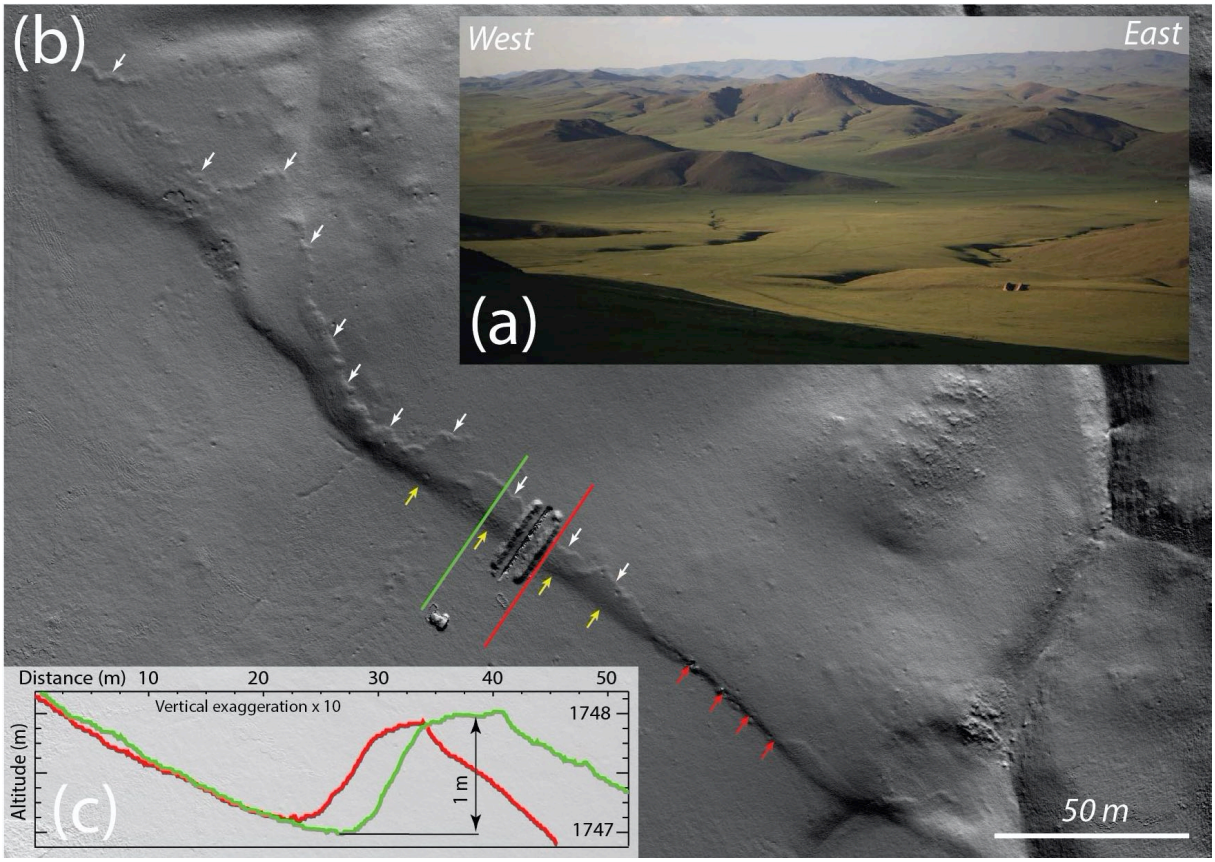

Figure 2: (a) Photograph of the trench and fault strand. (b) Shaded Digital Elevation Model of the scarp at the trenching site – derived from UAV images. The yellow, red arrows point respectively toward the main flexural fault scarp and a section where the rupture on the thrust reach the surface. The white arrows point toward the surface rupture of a secondary backthrust (c) Red and green topographic profiles through the Digital Elevation Model located on (b).

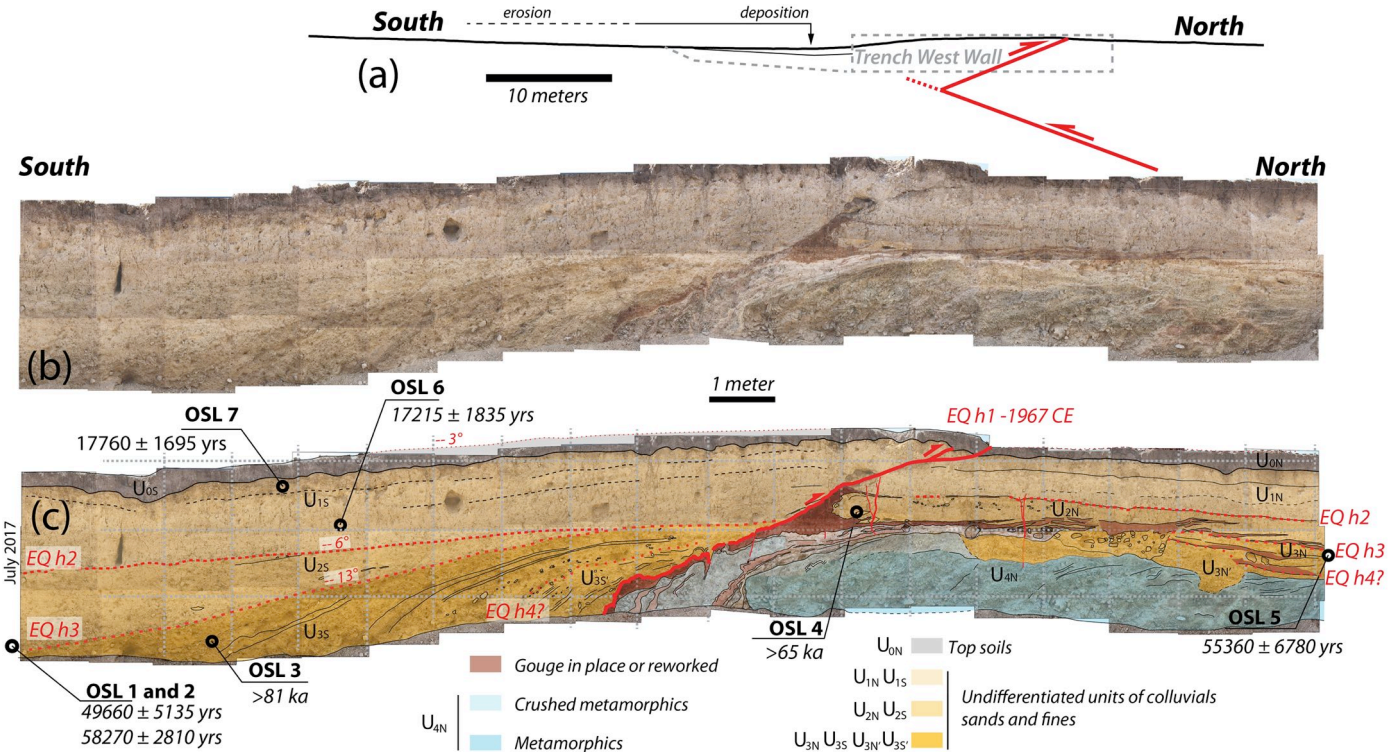

Figure 3: West Wall of the trench (a) Profile through the topography of Figure 2 and emplacement of the trench wall (b) Photomosaic and (c) Log of the west wall of the trench. July 2017. Minimum age Model OSL age from Table 1 are reported.

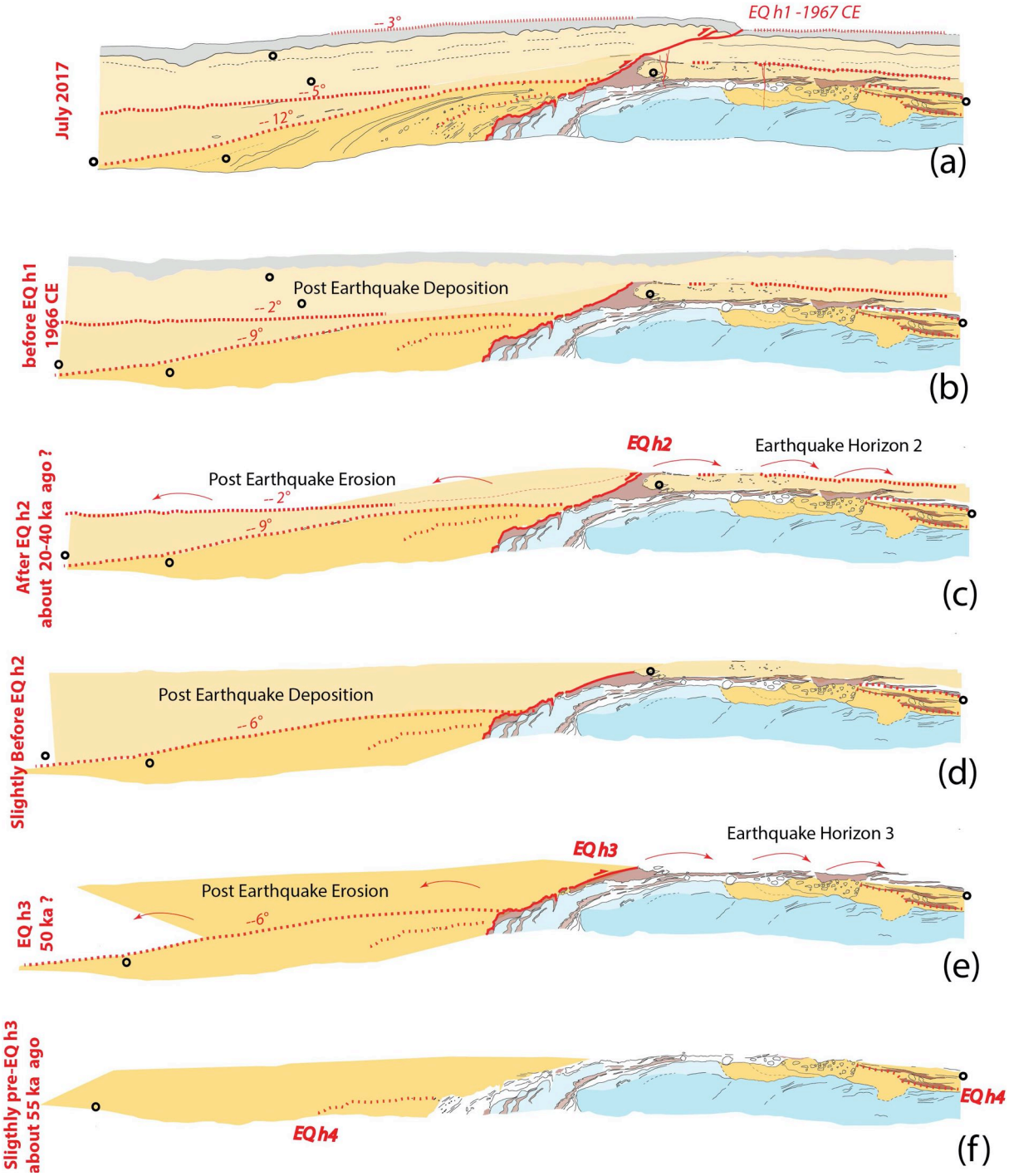

Figure 4: Schematic reconstruction. Incremental growth of the fold. Tilting of the frontal units.

Field number/depth (m)	Lab number	Aliquots[a]	Grain size (μm)	Finite Mixture D_e (Gy)[b]	Minimum Model D_e (Gy)[b]	Age Over-dispersion (%)[c]	U (ppm)[d]	Th (ppm)[d]	K (%)[d]	Cosmic Dose rate (mGray/yr)	Dose rate (mGray/yr)[d]	Finite Mixture OSL age (yr)[e]	Minimum Model OSL Age age (yr)[e]
MO17-OSL1	BG4574	5/50/60	250-150	146.12 ± 13.04	146.12 ± 13.04	37 ± 4	3.34 ± 0.01	6.98 ± 0.01	1.71 ± 0.01	0.22 ± 0.02	3.00 ± 0.06	48,650 ± 4310	49,660 ± 5135
MO17-OSL2	BG4579	11/36/40	250-150	156.90 ± 12.61	168.29 ± 6.41	31 ± 4	2.89 ± 0.01	6.98 ± 0.01	1.69 ± 0.01	0.22 ± 0.02	2.89 ± 0.15	54,370 ± 5195	58,270 ± 2810
MO17-OSL3	BG4576	20/23	150-100	>250		NA	2.11 ± 0.01	9.11 ± 0.01	1.87 ± 0.01	0.22 ± 0.02	3.08 ± 0.15	>81 ka	
MO17-OSL4	BG4578	36/40	250-150	>195		31 ± 4	1.37± 0.01	5.29 ± 0.01	2.40 ± 0.01	0.22 ± 0.02	3.02 ± 0.15	>65 ka	
MO17-OSL5	BG4575	6/31/31	250-150	149.22 ± 13.60	143.64 ± 17.64	31 ± 4	1.97± 0.01	6.18 ± 0.01	1.62 ± 0.01	0.25 ± 0.02	2.59 ± 0.14	57,500 ± 5370	55,360 ± 6780
MO17-OSL6	BG4573	6/47/51	250-150	39.50 ± 1.60	41.37 ± 4.29	61 ± 6	2.14 ± 0.01	5.04 ± 0.01	1.45 ± 0.01	0.25 ± 0.02	2.40 ± 0.06	16,440 ± 780	17,215 ± 1835
MO17-OSL7	BG4577	8/37/40	250-150	56.83 ± 2.21	50.45 ± 4.79	39 ± 5	2.41 ± 0.01	6.51 ± 0.01	1.73 ± 0.01	0.30 ± 0.03	2.84 ± 0.14	19,970 ± 885	17,760 ± 1695

[a]Aliquots measured, used and that define lowest most D_e population by Finite Mixture Model (Galbraith and Green, 1990).

[b]Equivalent dose calculated on a pure quartz fraction with ultra-small aliquots with 20-80 grains/aliquot and analyzed under blue-light excitation (470 ± 20 nm) by single aliquot regeneration protocols (Murray and Wintle, 2003). Equivalent dose (D_e) was calculated by the Finite Mixture Model (Galbraith and Green, 1990) and the four parameter Minimum Age Model (Gralbraith and Roberts, 2012).

[c] Overdispersion values reflects precision beyond instrumental errors; values of ≤ 25% (at 1 sigma limit) indicate low dispersion in equivalent dose values and a unimodal distribution. Values > 25% are associated with mixed equivalent dose signature reflecting multiple grain populations or partial solar resetting.

[d]U, Th, Rb and K content analyzed by inductively-coupled plasma-mass spectrometry analyzed by ALS Laboratories, Reno, NV; and includes dose contribution from Rb and a moisture content 5 ± 2%.

[e]includes also a cosmic dose rate calculated from parameters in Prescott and Hutton (1994) and includes soft components.

[e]Systematic and random errors calculated in a quadrature at one standard deviation by the Luminescence Dating and Age Calculator (LDAC) at https://www.baylor.edu/geosciences/index.php?id=962356. Datum year is AD 2010.

Table 1: Optically Stimulated Luminescence (OSL) ages on quartz grains sampled in the Mogod trenchsite. See suppl. Data material for methodology and references.

461

Figures

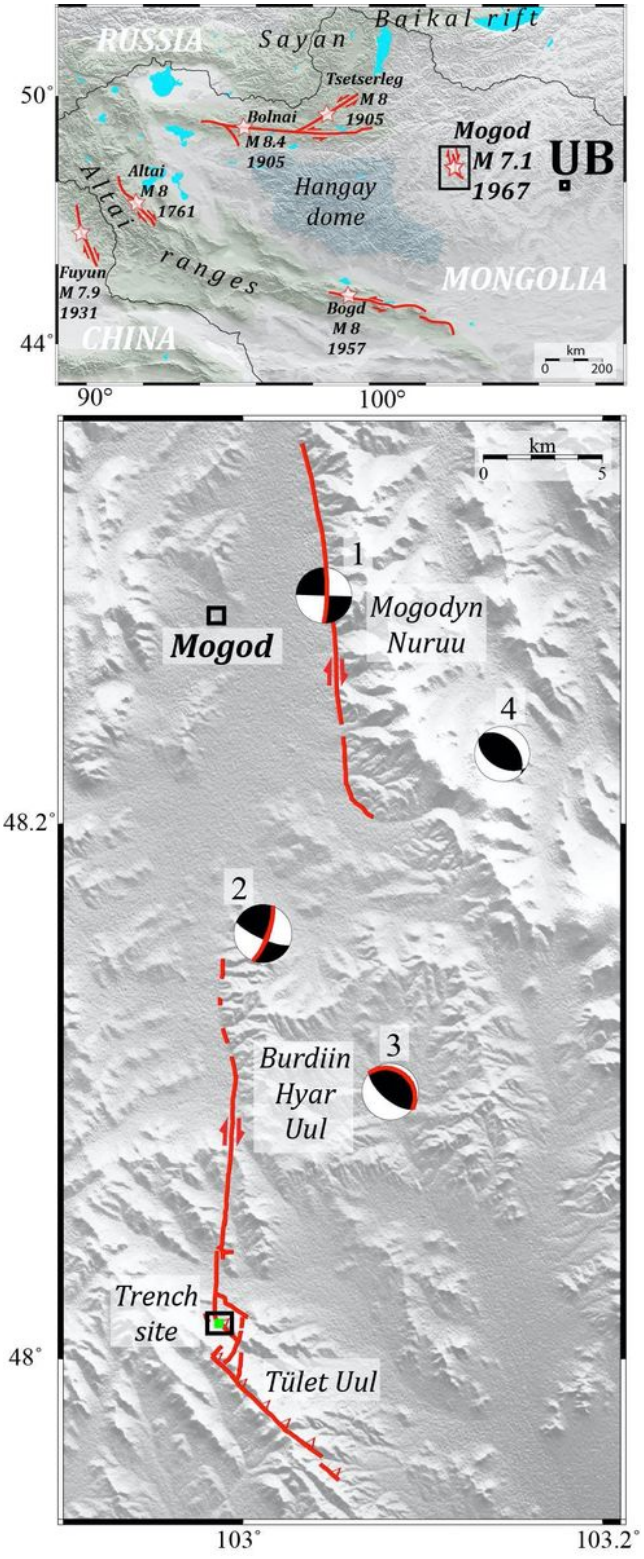

Figure 1

please see the manuscript file for the full caption

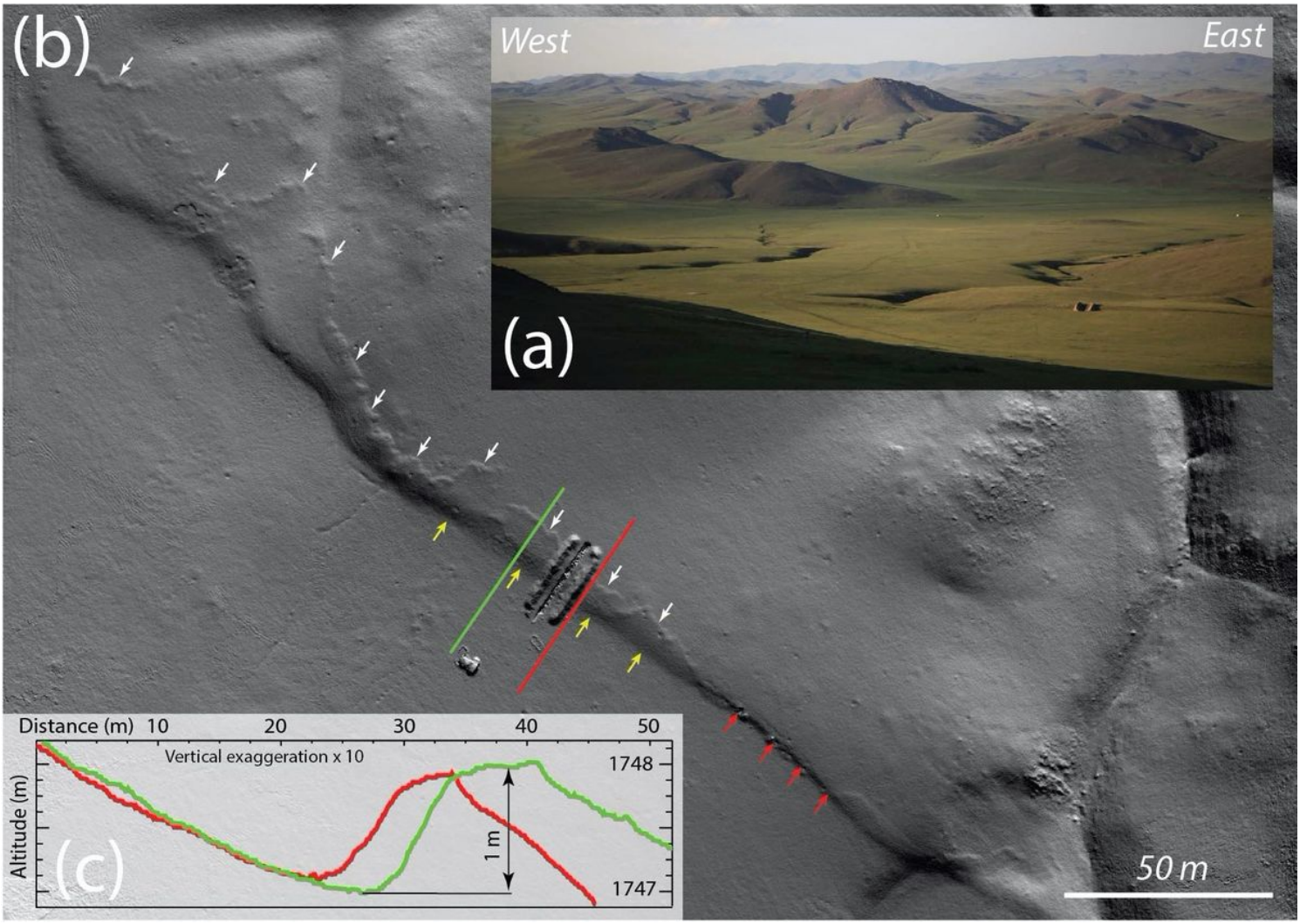

Figure 2

please see the manuscript file for the full caption

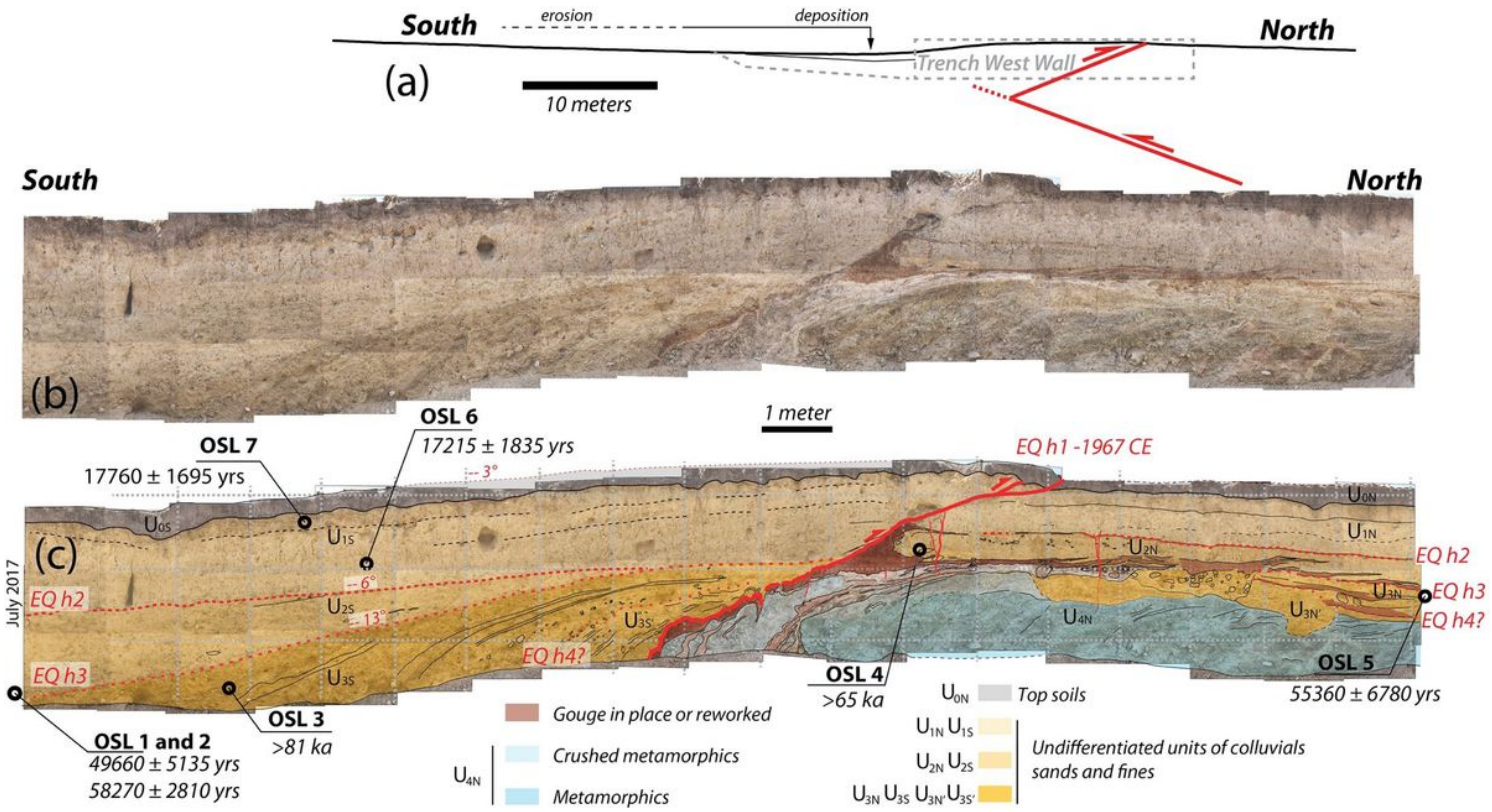

Figure 3

please see the manuscript file for the full caption

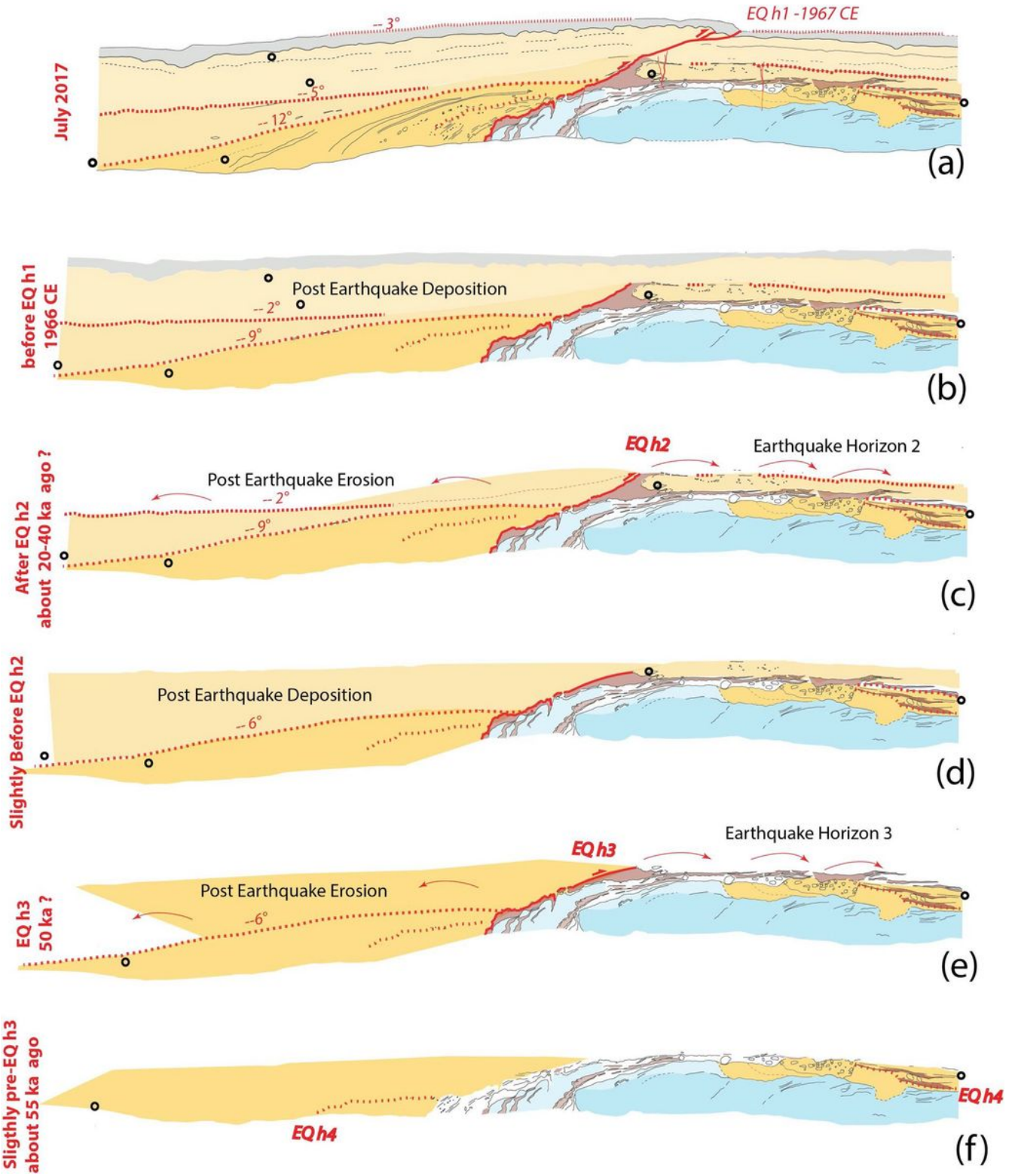

Figure 4

please see the manuscript file for the full caption

Supplementary Files

This is a list of supplementary files associated with this preprint. Click to download.

- Bollinger2021supplementarydata.docx